Intermetallics 52 (2014) 15–19

Contents lists available at ScienceDirect

Intermetallics

journal homepage: www.elsevier.com/locate/intermet

Anisotropic nanocrystallization of a Zr-based metallic glass induced by Xe ion irradiation

H.C. Chen [a], L. Yan [a,*], R.D. Liu [a], M.B. Tang [b], G. Wang [c], H.F. Huang [a], Y. Hai [a], X.T. Zhou [a,**]

[a] Shanghai Institute of Applied Physics, Chinese Academy of Sciences (CAS), 2019 Jialuo Rd., Jiading, Shanghai 201800, China
[b] Key Laboratory of Transparent and Opto-functional Inorganic Materials, Shanghai Institute of Ceramics, Chinese Academy of Sciences, Shanghai 200050, China
[c] Laboratory for Microstructures, Shanghai University, Shanghai 200444, China

ARTICLE INFO

Article history:
Received 27 November 2013
Received in revised form
12 March 2014
Accepted 15 March 2014
Available online 9 April 2014

Keywords:
B. Glasses, metallic
B. Anisotropy
C. Nanocrystals
F. Electron microscopy, transmission
F. Ion-beam methods

ABSTRACT

Structural modification in a Zr-based metallic glass caused by irradiation with 7 MeV Xe^{26+} ions was investigated. Needle-like nanocrystalline structures, formed under ion irradiation, consist of $Cu_{10}Zr_7$ phase (primary) and/or minor $(Ni_xCu_{1-x})_{10}Zr_7$ phase. The formation of needle-like nanocrystals suggested an anisotropic atomic diffusion caused by ion irradiation.

1. Introduction

Metallic glasses have been a subject of great interest during the past decades because of their unique mechanical and chemical properties, such as high specific strength [1] and good corrosion resistance [2]. Generally, metallic glasses are metastable. However, a phase transformation and/or crystallization can occur when an amorphous phase was exerted by external energies, such as mechanical energy and heat energy [3,4], etc. Numerous studies have shown that the formation of crystalline structure can be induced and/or effected by annealing [5], deformation [6,7], bending [8], nanoindentation [9], magnetic field [10], and particle irradiation [11–13], etc. Recently, it has been found that some metallic glasses with nanocrystalline structures exhibited excellent properties. For instance, a Zr–Al–Cu-based metallic glass with nanocrystalline structure has higher tensile strength and better ductility than those of the monolithic metallic glasses [14]. In addition, a Fe-based amorphous alloy containing nanocrystalline α-Fe phase can yield desirably soft magnetic properties [15].

It is well known that ion irradiation can improve the atomic mobility and enhance the crystallization process [11]. According to the free volume concept [16,17], enhanced atomic mobility can lead to order structure and crystallization in the amorphous phase at a relative low temperature. Under irradiation, displacement by energetic particles can increase the free volume within the system and enhance atomic mobility. Therefore, particle irradiation technique is expected to lead to order structure and subsequent crystalline nucleation in a metallic glass system.

Zr-based metallic glasses have widespread practical applications [18]. However, little is known about the radiation effects on Zr-based metallic glasses. In this work, we choose $Zr_{50.7}Al_{12.3}Cu_{28}Ni_9$ metallic glass as a model material to investigate the influence of ion irradiation on the microstructure of this metallic glass. It can be found that some needle-like nanocrystalline structures are formed under ion irradiation.

2. Experimental methods

Alloy ingots with nominal compositions of $Zr_{50.7}Al_{12.3}Cu_{28}Ni_9$ were prepared by arc melting the mixtures of pure metals under a Ti-gettered argon atmosphere, followed by suction casting into copper molds to form rod-like bulk metallic glass samples with a size of Φ 3 mm. For Transmission electron microscopy (TEM) observation, thin foils cut from the rod-like samples were

* Corresponding author. Tel.: +86 21 39194773.
** Corresponding author.
E-mail addresses: chenhuaican@sinap.ac.cn (H.C. Chen), yanlong@sinap.ac.cn (L. Yan), zhouxingtai@sinap.ac.cn (X.T. Zhou).

http://dx.doi.org/10.1016/j.intermet.2014.03.006
0966-9795/

mechanical polished from the plates to be about 100 μm in thickness, and then, twin jet polishing in a solution of 5% perchloric acid and 95% alcohol at 243 K was used to make electron transparent samples [19].

The ion irradiation of the thin foils for TEM observation was carried out with Xe^{26+} ions at room temperature in a terminal of 320 kV High-Voltage Experimental platform equipped with an electron cyclotron resonance ion source in Institute of Modern Physics, Lanzhou, China. The energy of Xe^{26+} ion was fixed at 7 MeV. The incident flux was about 2×10^{11} ions/cm^2 s and achieved a total fluence of 6×10^{15} ions/cm^2. The vacuum was kept below 5×10^{-5} Pa during ion irradiation. TEM and high-resolution TEM (HRTEM) were performed in a FEI Tecnai G^2 F20 microscope, operated at 200 kV.

3. Results and discussions

Fig. 1(a) and (b) shows a TEM bright-field (BF) micrograph and a HRTEM micrograph of an unirradiated sample, respectively. The inset of Fig. 1(a) is the corresponding selected area electron diffraction (SAD) pattern. No evidences of crystalline phases and precipitations are observed. The presence of a very diffuse and broad halo in the SAD pattern reveals that the alloy is in a fully amorphous state, which is in accordance with the result of HRTEM (Fig. 1(b)).

Fig. 2(a) and (b) shows TEM-BF image and corresponding TEM dark-field (DF) image of the Xe^{26+} irradiated sample with the irradiation dose of 6×10^{15} ions/cm^2, respectively. Fig. 2(c) and (d) are the enlarged TEM-BF image and corresponding TEM-DF image of the needle-like precipitations, respectively. Some needle-like precipitations with a length of 100–200 nm and a width of 5–10 nm, and some particles with diameter of 10–50 nm are clearly observed. The average area proportion of these precipitations is up to 43%. Fig. 2(e) shows the HRTEM image of the needle-like precipitation obtained from the white square area in Fig. 2(c). The corresponding fast Fourier transformation (FFT) pattern and the inverse Fast Fourier Transformation (IFFT) image by the white square area in Fig. 2(e) are shown in Fig. 2(f) and (g), respectively. The observed diffraction spots and lattice fringes are clear evidence for the formation of nanocrystalline. Thus, we understand the needle-like precipitations are nanocrystals.

Fig. 3 shows TEM-BF image of the irradiated sample and corresponding the corresponding SAD pattern. In Fig. 3(b), SAD pattern shows the sharp rings overlapped by some diffraction spots, which indicates the formation of nanocrystals. The calculated interplanar distances in this study are compared with those from database [20] in Table 1. Silicon single crystal with the crystalline plane of (100) is used for calibration. The experimentally measured d-spacing points to the standard d-spacing of $Cu_{10}Zr_7$ and $Ni_{10}Zr_7$ phase. The d-spacing of 2.890 Å can be exclusively assigned to the (311) plane from $Cu_{10}Zr_7$. Thus, the observed primary crystalline phase in Fig. 3(a) should be $Cu_{10}Zr_7$, because the diffraction ring corresponding to the (311) plane of $Cu_{10}Zr_7$ is bright and sharp. However, it is difficult to confirm the existence of $Ni_{10}Zr_7$ phase. Actually, the similarity between Ni and Cu in electronegativity (1.91 and 1.9) and atomic radius (0.135 nm and 0.128 nm) [21] coupled with the similar stoichiometry of $Cu_{10}Zr_7$ and $Ni_{10}Zr_7$ and orthorhombic structures may imply the mutual solubility of $Ni_{10}Zr_7$ and $Cu_{10}Zr_7$. This suggests the formation of $(Ni_xCu_{1-x})_{10}Zr_7$ phase structure. The similar type of substitutional intermetallic structure was reported in Zr–Al–Cu–Ni and Fe–Cr–Ni–Zr alloy systems [22,23]. Thus, it is suggested that the crystalline phases should contain $Cu_{10}Zr_7$ phase (primary) and/or minor $(Ni_xCu_{1-x})_{10}Zr_7$ phase.

Fig. 4(a) shows high-angle annular dark field scanning transmission electron microscope (HAADF-STEM) image of Xe^{26+} ion irradiated sample, the needle-like precipitations are also observed, which is consistent with bright-field image (in Fig. 2(a)). According to the Pennycook's theory [24–27], atomic number- (Z-)contrast imaging principle can be formulated by the followed equation.

$$I_s = \left(\frac{m}{m_0}\right) \frac{Z^2\lambda^4}{4\pi^3\alpha_0^2} \left(\frac{1}{\theta_1^2 + \theta_0^2} - \frac{1}{\theta_2^2 + \theta_0^2}\right) NtI$$

where I_s is the scattering intensity, I is the electron intensity, m is high energy electron mass, m_0 is electron rest mass, Z is atomic number, λ is electron wavelength, α_0 is Bohr radius, N is the number of atom in unit volume, t is thickness of the sample, $\theta_{0,1,2}$ is the special parameter. The equation indicates that the intensity of HAADF is in directly proportional to the square of atomic number. That is, the contrast of the HAADF image is the function of atomic number. The white contrast of the precipitates in Fig. 4(a) shows the enrichment of heavy atomic number elements compared with matric with gray contrast region, which suggests the enrichment of Zr and/or Cu should be observed by STEM-EDS.

Fig. 4(d) and (f) shows enlarged STEM-HAADF image and corresponding STEM-EDS line scan, respectively. In Fig. 4(f), the black dash curve is the spectrum of HAADF detector, the other curves are the spectrums of various elements as the function of the position. The area between the dot lines is corresponded with the needle-like crystal area in Fig. 4(d). The observed enrichment of Zr element in needle-like crystal area confirms that the precipitates

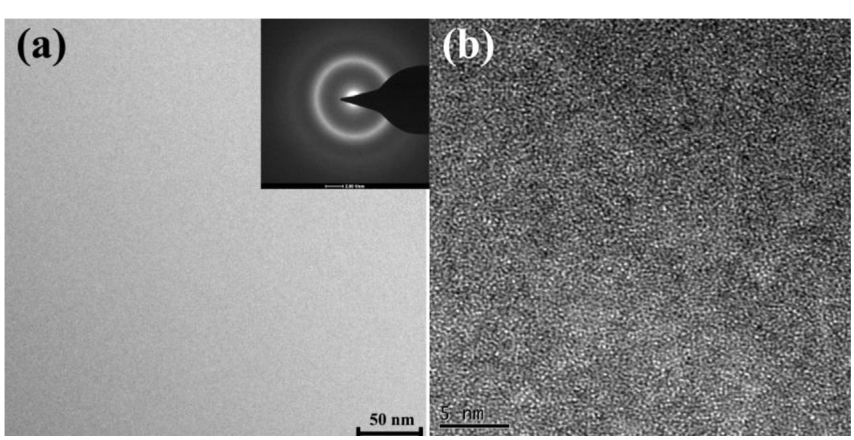

Fig. 1. (a) Bright-field TEM micrograph, and (b) HRTEM micrograph of unirradiated $Zr_{50.7}Al_{12.3}Cu_{28}Ni_9$ metallic glass. The corresponding SAD pattern in inset.